Bulletin of the Seismological Society of America, Vol. 75, No. 2, pp. 427–439, April 1985

DETERMINATION OF ELASTIC WAVE VELOCITY AND RELATIVE HYPOCENTER LOCATIONS USING REFRACTED WAVES. II. APPLICATION TO THE HAICHENG, CHINA, AFTERSHOCK SEQUENCE

By Kaye M. Shedlock, Lucile M. Jones, and Ma Xiufang

Abstract

We located the aftershocks of the 4 February 1975 Haicheng, China, aftershock sequence using an arrival time difference (ATD) simultaneous inversion method for determining the near-source (*in situ*) velocity and the location of the aftershocks with respect to a master event. The aftershocks define a diffuse zone, 70 km x 25 km, trending west-northwest, perpendicular to the major structural trend of the region. The main shock and most of the large aftershocks have strike-slip fault plane solutions. The preferred fault plane strikes west-northwest, and the inferred sense of motion is left-lateral. The entire Haicheng earthquake sequence appears to have been the response of an intensely faulted range boundary to a primarily east-west crustal compression and/or north-south extension. The calculated upper mantle *P*-wave velocity is 7.6 ± 0.09 km/sec, and the inferred crustal thickness is between 31 and 32.5 km. The low upper mantle velocity and thin crust may be indicative of local lithospheric extension.

Introduction

The Haicheng earthquake (M_S = 7.3) struck Liaoning province, northeastern China on 4 February 1975. This earthquake was the third of four large ($M_S > 7.0$) strike-slip earthquakes to occur in the North China basin region (within approximately 850 km of one another) between 1966 and 1976. The North China basin is the second largest of the more than 40 Mesozoic-Cenozoic basins distributed throughout eastern China (Tang, 1982). Formed during the Cenozoic, this NE-SW trending sedimentary basin is comprised of several smaller depressions with different histories of crustal extension (Ye *et al.*, 1985). The Haicheng earthquake occurred near the flank of the northeasternmost smaller depression, the Xialiao depression (Figure 1) and was most unusual in that the main shock ocurred beneath the Liaodong Mountains. The aftershock zone, however, extended out into the basin. Based on the fault plane solution and the shape of the aftershock zone, it appears that the main shock occurred on a west-northwest striking fault perpendicular to the major structural trend of the region.

The Haicheng aftershocks provide an excellent opportunity to study the crust and upper mantle structure of the North China basin region, an area about which little is known. The entire earthquake sequence was recorded by a permanent array of seismic stations supplemented by a temporary array of stations to record the foreshock activity. We applied a simultaneous hypocenter location-velocity inversion method using direct and refracted wave arrivals (Shedlock and Roecker, 1985) to 135 events of the aftershock sequence in order to determine the *in situ* velocity structure and to examine the distribution of faulting.

This study is part of the Earthquake Studies Protocol between the United States of America and the People's Republic of China. The agreements contained in the Protocol facilitated our access to earthquake records belonging to both Liaoning and Shandong provinces in northeastern China.

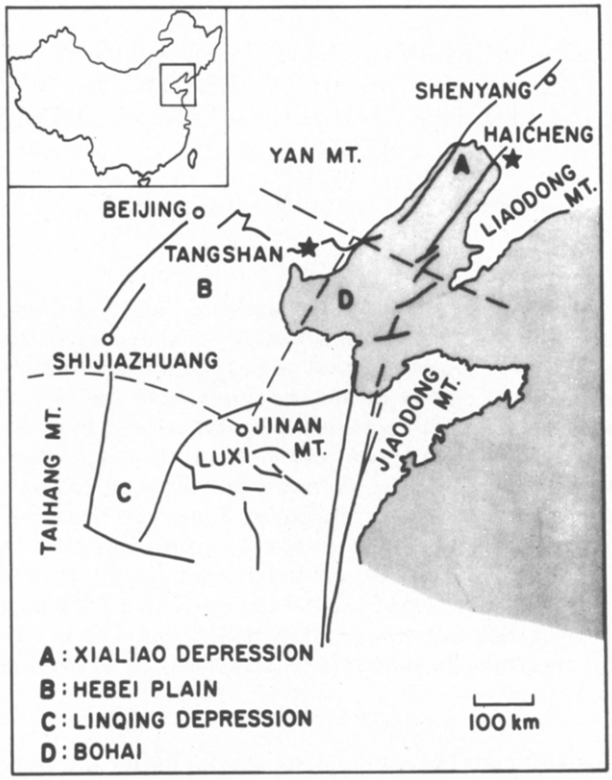

FIG. 1. The North China Basin with four interior areas of major depressions delineated by broken lines. Solid lines are faults, stars are earthquakes, and circles are cities. *Shaded area* is offshore.

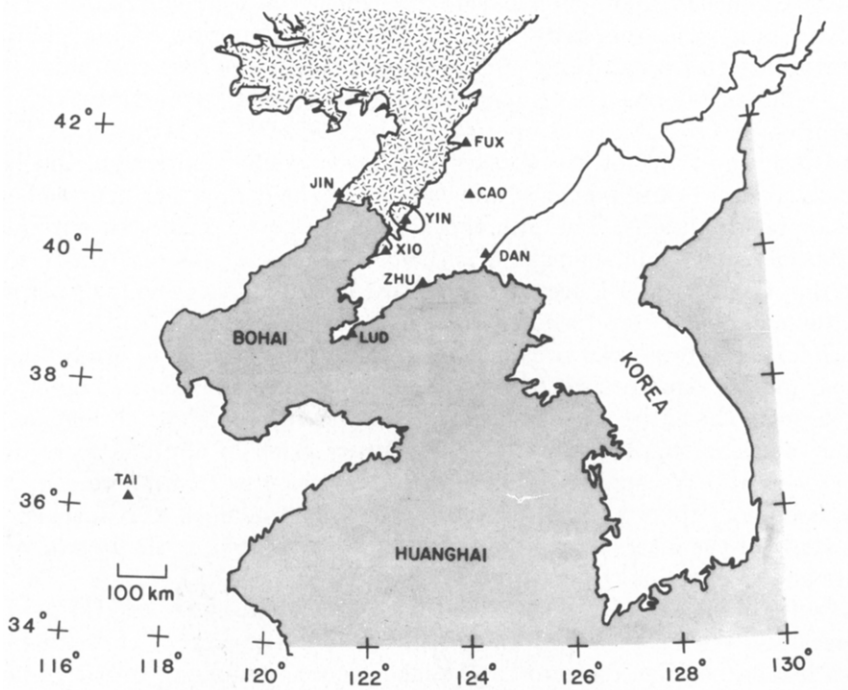

FIG. 2. Distribution of stations used in this study. The *stippled area* denotes the Quaternary and Tertiary alluvial deposits of the Xialiao depression. The ellipse around YIN denotes the aftershock zone.

DATA

Thousands of aftershocks associated with the Haicheng earthquake occurred between 4 February 1975 and 30 June 1980. Seismic activity was nearly continuous for approximately 30 hr after the main shock. The earliest aftershock for which clear arrivals could be picked at several stations occurred on the 6 February. We measured P_n, P, S_n, and S arrival times at as many as nine stations for 135 aftershocks.

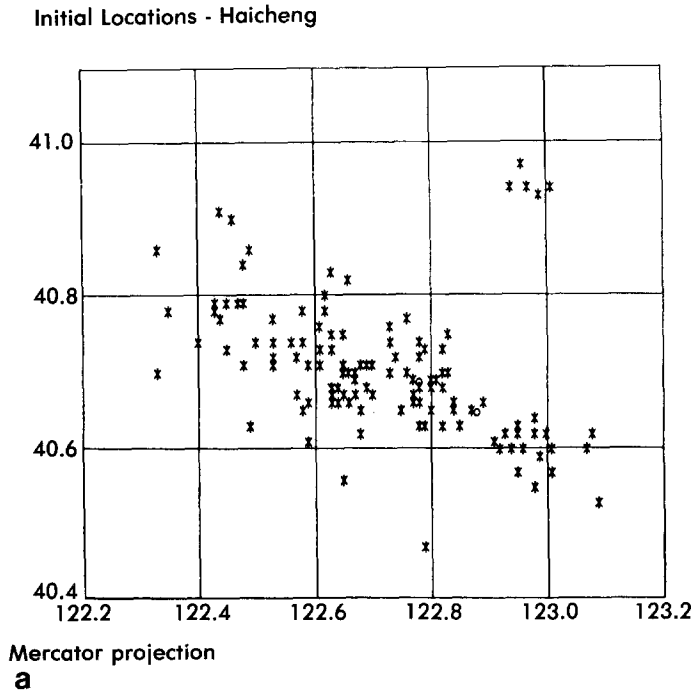

FIG. 3. (a) Map view of the locations of all 135 aftershocks. Stars denote depths ≦ 16 km, open circles > 16 km. (b) Cross-section of the aftershock locations. The aftershocks are projected onto a plane striking N68°W through the point 40.6° latitude, 122.8° longitude. The plotting routine we used plots events with negative depth (above ground locations) on the surface.

Eight of the stations used in this study are operated by the Liaoning Provincial Seismology Bureau and the ninth, TAI, is operated by the Shandong Provincial Seismology Bureau (Figure 2). Station XIO was not in operation during February 1975, and CAO was a portable station that was dismantled at the end of March 1975. At all of the stations, three-component short-period instruments were recorded

on smoked paper. At each recording site, the differences between the station clock and WWVH radio time was measured daily with a stopwatch, introducing errors in individual measurements as large as 0.5 sec. To reduce the error in the clock correction at each station, we fitted a straight line (or a smooth curve) to the deviations measured during an interval of 4 days preceding and following each event. We then interpolated these curves to determine the clock corrections for each arrival time. This reduces the error due to clock correction to about 0.1 sec (Jones *et al.*, 1982).

We calculated initial absolute locations for each aftershock with two different computer programs: BERQ85 (Evernden, 1980) and HYPOINVERSE (Klein, 1978), using the crustal structure in Table 1. These initial locations defined an elliptical, northwest-trending aftershock zone roughly 30 km wide by 90 km long with a

TABLE 1

INITIAL VELOCITY MODEL (LIAONING PROVINCIAL SEISMOLOGY BUREAU)

Layer	V_p (km/sec)	Thickness (km)
1	6.0	16.0
2	7.0	15.0
half-space	8.0	∞
	Final Velocity Model	
Layer	V_p (km/sec) (±S.E.)	Thickness (km)
1	5.71 ± 0.07	16.0
2	6.63 ± 0.07	15.0
half-space	7.60 ± 0.08	∞
	Model B	
Layer	V_p (km/sec) (±S.E.)	Thickness (km)
1	5.50 ± 0.06	4.0
2	6.00 ± 0.08	13.0
3	6.60 ± 0.08	15.5
half-space	7.60 ± 0.09	∞

separate, smaller cluster of aftershocks about 20 km to the northeast (Figure 3a). The initially calculated hypocenter depths were very shallow, with several events locating above ground (Figure 3b). The average root-mean-square (rms) travel-time residual was 0.58 sec with an associated average error ellipse of 1.7 x 3.8 km (horizontal x vertical semi-major axes).

Station by station examination of the travel-time residuals for each event revealed two consistent patterns. First, the residuals generally increased with epicentral distance. Both this observation and the shallow depths suggested that the assumed velocities were too high. Second, the travel-time residuals for refracted phases were smaller than the residuals for direct phases. We decided to use a simultaneous inversion method that uses both refracted and direct arrivals to relocate the aftershocks and to refine the velocity structure.

METHOD

Simultaneous inversion methods are widely used to determine the hypocentral locations and velocity structure surrounding earthquake sequences (e.g., Fitch, 1975; Crosson, 1976; Aki and Lee, 1976; Thurber, 1981; Roecker, 1982). We used a

simultaneous inversion method developed expressly for cases in which most first arrivals followed refracted paths. The formulation and testing of this method are discussed in Shedlock and Roecker (1985), but we include a brief summary here. This simultaneous inversion method, an arrival time difference (ATD) method (Fitch, 1975), is based on the assumption that the earth structure in the source region may be represented by homogeneous velocity layers over a half-space. The difference in arrival times between a master and secondary event to each station are assumed to be primarily due to path differences near the source rather than near the individual receivers. Thus, this method obviates the need for station corrections. The arrival time differences between the pairs of events to the stations are minimized by an iterative scheme that uses the method of parameter separation (Pavlis and Booker, 1980) to locate the events with respect to a master and to adjust velocities of the layers in the initial crustal model.

Application

The aftershocks were divided into three groups for the simultaneous inversion process. One group had a different station configuration than the other two since station DAN was moved in December 1975. The wide geographic distribution of the remaining aftershocks led us to divide them into two overlapping groups, each with a corresponding master event. The overlap of events allowed us to be sure that the locations were consistent, regardless of which master was used. The grouping of aftershocks allowed over 80 per cent of the aftershocks to be located.

We used only those aftershocks with rms travel-time residuals $\leqq 0.5$ sec in the simultaneous inversion. The aftershocks were first located with respect to a master event. The travel-time residuals from these locations were then minimized by performing an inversion for near-source velocity. Then, using the corrected velocity model, the aftershocks were relocated with respect to a master event. These iterations continued until terminated by an F-test comparison of the ratio between the rms travel-time residual before and after each iterative step (DeGroot, 1975). This comparison guaranteed that the iterations continued until no significant change was made in the velocity model. Since this simultaneous inversion method holds the interface depths constant, we also inverted for velocity with combinations of interface depths, using both the originally assumed values of velocity and the final values (Table 1).

All three groups of aftershocks converged to the same velocity model and standard errors (Table 1). The average rms travel-time residual for the aftershocks located using the final velocity model was 0.26 sec, less than half the average residual calculated using the initially assumed model. The average error ellipse was 1.0×2.1 km. Although the rms travel-time residual of 0.26 sec associated with the final velocity model was the minimum, there were several others with residuals close to this minimum (Figure 4). We tested combinations of interface depths by holding the depths constant and applying the simultaneous inversion method to each combination. For deeper mid-crustal interfaces, the uncertainty associated with the velocity of the upper layer increased while velocity uncertainties of the lower layer and half-space decreased or remained unchanged. Thus, we decided to test some three-layer combinations. Since the rms travel-time residuals for different assumed velocity structures often differed by only 0.01 to 0.02 sec, we also used resolution of the model (see Aki and Richards, 1980), and reduction in the size of the average error ellipse associated with the locations to decide upon the final model. All of this

testing yielded a second velocity model (model B, Table 1) with nearly the same rms residual (0.28 sec) as the final model and an average error ellipse only 9 per cent larger than that of the final model. However, the resolution matrix for model B had smaller diagonal elements and larger off-diagonal spread than that of the resolution matrix for the chosen final model. While interpretation of resolution matrices is somewhat qualitative, we chose the final model, listed in Table 1, both because of the larger diagonal elements of the resolution matrix and because of the smaller error ellipses associated with the earthquake locations.

In this study only the P-wave velocities in each layer were determined by the inversion. S waves, however, were used to stabilize the earthquake locations. The corresponding S-wave velocities were constrained assuming the relationship $V_p/V_s = 1.73$, obtained for the Haicheng aftershocks using Wadati diagrams.

All of the aftershocks were relocated both relatively and independently using the

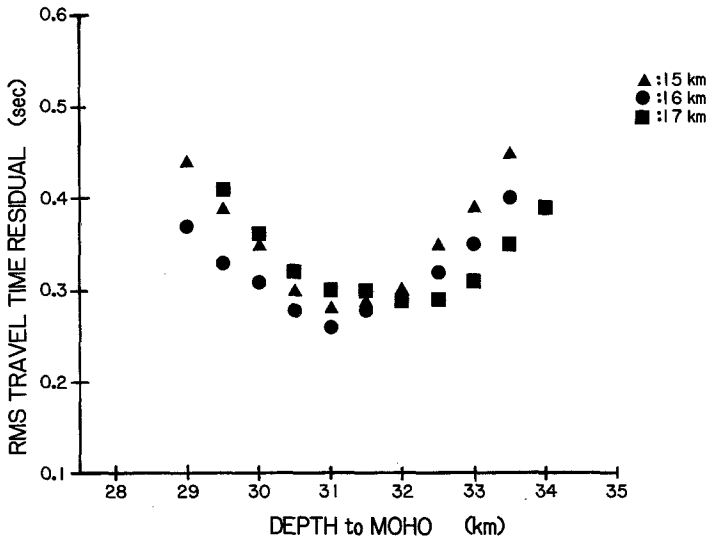

FIG. 4. Plot of rms travel-time residuals versus depth to Moho. The symbol indicates depth to the upper interface.

final velocity model. In general, the epicenters calculated using these two methods for each event differed by less than 0.05°, but there was greater spread in the depths. The error ellipsoids associated with the relative relocations were smaller, by a factor of 2 in depth and a factor of nearly 5 in epicenter than those of the ellipsoids associated with the independent locations. Of the 135 aftershocks, the locations of 87 aftershocks (64 per cent) were considered to be well-constrained (Figure 5) according to the following criteria.

1. rms travel-time residual $\leqq$ 0.4 sec,
2. the probability of the hypocenter lying within an ellipsoid with major axes of standard horizontal error $\leqq$ 1.0 km and standard vertical error $\leqq$ 3.0 km is calculated to be 95 per cent or greater.

DISCUSSION

The 4 February 1975 Haicheng earthquake occurred in a geologically complex intracratonic region. The main shock occurred near the transition between the Xialiao depression and the Jiaoliao uplift in northeastern China (Figure 1). The

Xialiao depression, the northeasternmost depression in the North China Basin group, is a faulted, sediment-filled northeast-southwest trending depression, which began forming in early to middle Eocene time. It is currently 65 km wide and as deep as 6 km (Shedlock *et al.*, 1985). The Xialiao depression is flanked by the Yan Mountains to the northwest and the Liaodong Mountains to the southeast. The Jiaoliao uplift (the Liaodong and Jiaodong Mountains), which also trends northeast-southwest, is comprised of Archean and Proterozoic schist and gneiss intruded

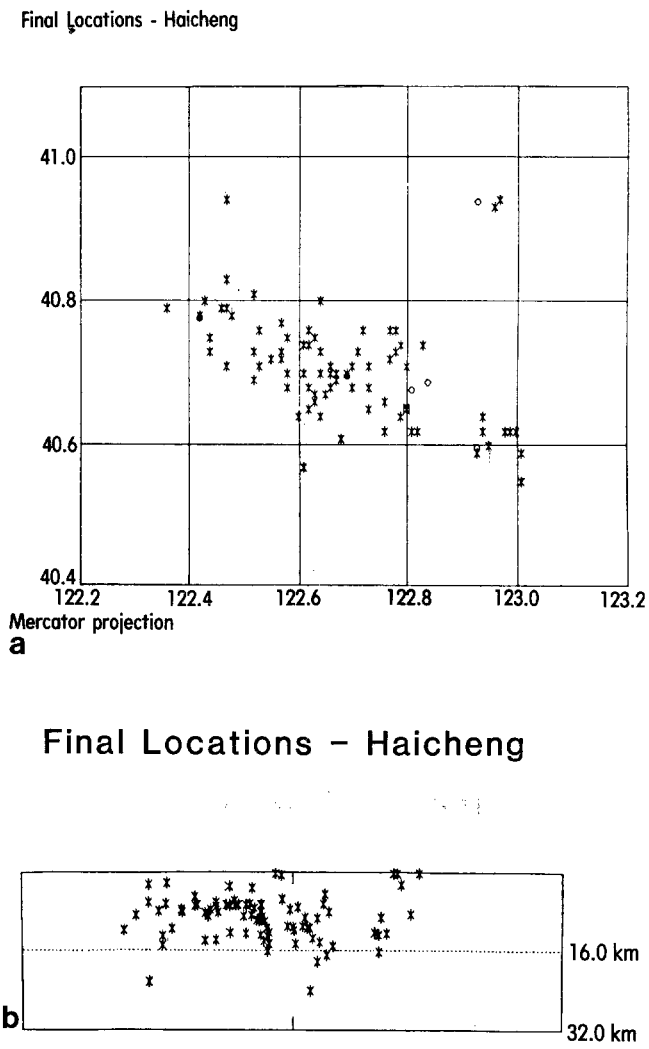

FIG. 5. (a) Map views of the 87 well-located aftershocks. Same symbol convention as in Figure 3a. (b) Cross-section of the well-located aftershocks. Same projection as in Figure 3.

by Mesozoic granitic batholiths. Delineation of faults in the region is complicated by the thick sedimentary cover in the depression and the absence of identifiable features in the strongly metamorphosed schist and gneiss. The general northeast-southwest trend of major tectonic features is also reflected by mapping of Tertiary and Quaternary faults (Figure 6). The Tanlu fault zone, an approximately 2000-km-long fault zone, passes from the northeast to the southwest through the Xialiao depression as four subparallel faults. Features offset by the faults imply Quaternary

dextral strike-slip along the Tanlu fault system in southern Shandong Province (Fang *et al.*, 1976), but the thick sedimentary cover in the Xialiao depression obscures the fault to the northeast making similar observations there impossible. The majority of the smaller faults mapped near the Tanlu system also trend northeast-southwest. However, the fault plane solution determined both from first motion data (Wu *et al.*, 1976; Gu *et al.*, 1976; Hsu, 1976; Figure 7), and a synthesis of long-period *P* waves (Cipar, 1979) and the aftershock distribution seem to indicate that the Haicheng main shock occurred on a west-northwest trending fault. The fault plane solution of the mains shock inferred from first motions by Gu *et al.* (1976) describes a fault plane striking N70°W while that of Wu *et al.* (1976) and Hsu (1976) gives a N68°W striking fault plane. Waveform modeling by Cipar yielded a N72°W striking main shock fault plane.

The aftershock zone generally trends west-northwest (Figure 6), but it echos the

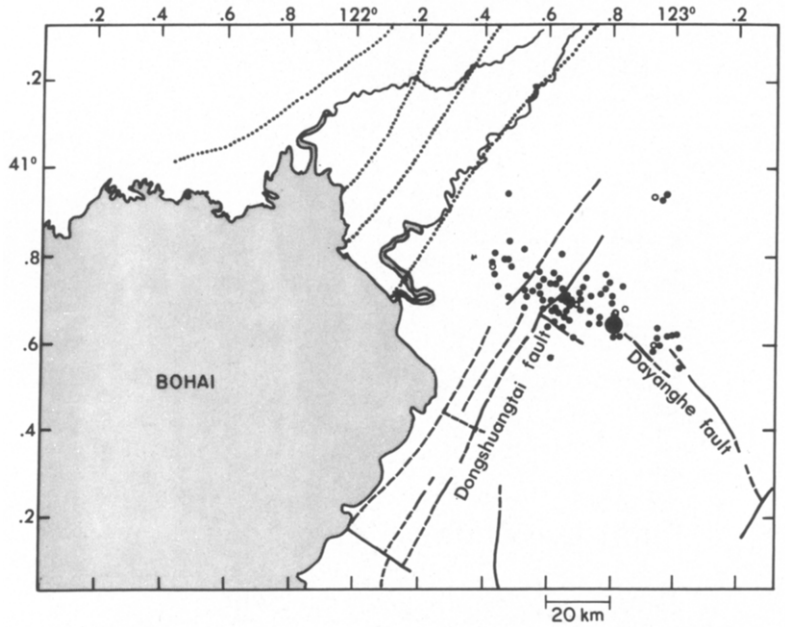

FIG. 6. Recently active (Quaternary and Tertiary) faults and well-located aftershocks. Solid circles are aftershocks ≦ 15 km deep; open circles are aftershocks > 15 km deep. The large solid circle denotes the main shock. The dashed lines are inferred faults. The dot-dashed lines are the four faults of the Tanlu fault system.

complexity of the mapped fault traces. The general west-northwest trend of the aftershock zone is subparallel to the accepted fault plane of the main shock, but the Haicheng aftershock zone is somewhat diffuse with no clear interior trends of seismic activity. The diffuse nature and large areal extent of the aftershock zone suggests movement on several neighboring faults, some of which may be more consistent with the prevailing northeast-southwest structural trend.

The aftershock zone is elliptical in shape, approximately 70 km x 25 km. Inclusion of the three events northeast of it (Figure 4) increases the width to about 45 km. Calculated depths range from near surface to 24 km, but 93 per cent of the aftershocks are shallower than 15 km (Figure 5). Some west-northwest trending faults are mapped near the epicenter of the main shock, most notably the Dayanghe (Figure 6). In fact, the southeast cluster of events from the aftershock zone appears

to be as much associated with the tip of the southeastern section of the Dayanghe as with the presumed main shock fault plane. The main shock is located near the northeast tip of the western mapped section of the Dayanghe fault, but the strikes of both strands of the Dayanghe fault are approximately N45°W, significantly different from the N70°W striking fault plane of the main shock (Figure 7). Thus, the main shock probably occurred on an unmapped fault with a more westerly strike than the Dayanghe fault (Jones *et al.*, 1982). There is no consistent trend of epicenters, either parallel to N70°W or other mapped faults. That the aftershocks do not clearly define the main shock fault plane is not without precedent in extensively faulted areas (Soufleris *et al.*, 1982; King and Yielding, 1984). Aftershocks should occur where stress has been increased by the main shock e.g., on the small, subparallel, and transverse faults and at any asperities on the main shock fault plane.

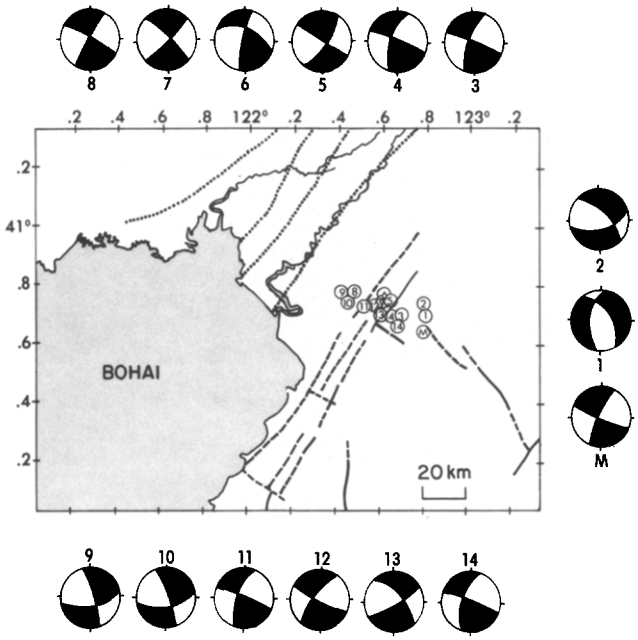

FIG. 7. Lower hemisphere fault plane solutions of the main shock (M) and most aftershocks with $M_S \geqq 4.0$. The black quadrants are compressional and the white quadrants are dilatational. Locations plotted were determined by this study.

Fault plane solutions of some of the larger aftershocks are similar to that of the main shock (Figure 7). The entire Haicheng earthquake sequence appears to have been the response of an intensely faulted region to approximately east-west crustal shortening or north-south extension. Two of the large aftershocks (9 and 10 in Figures 7 and 8) were initially located along the ~N70°W trend of the entire zone. This lead Gu *et al.* (1976) to initially interpret these events as having reverse polarity focal mechanisms with respect to the main shock in response to overshoot along the fault zone during the main shock. However, the hypocentral relocations of these two aftershocks places event 10 south-southeast of event 9. These locations would be consistent with an unmapped left-lateral, strike-slip fault rupturing along the north-northwest trending nodal plane. This sense of motion is also consistent with the overall sense of regional strain. The fault plane solutions of two other

aftershocks (1 and 2 in Figures 7 and 8) show normal faulting. The epicenters of both events are north of the main shock and probably also reflect the responses of other structures to the change in the prevailing stress field.

The layer velocities found for the final velocity model are 5.7 km/sec for the upper crust, 6.6 km/sec for the lower crust, and 7.6 km/sec for the upper mantle (Table 1) and are roughly 5 per cent less than those of the starting model. Station TAI (Figure 2) is far enough away that all paths from the aftershock zone to TAI were refracted at the Moho. Initially, the differences between the observed and calculated travel times were so large that readings from TAI were consistently rejected by the simultaneous inversion scheme. Nevertheless, with each velocity

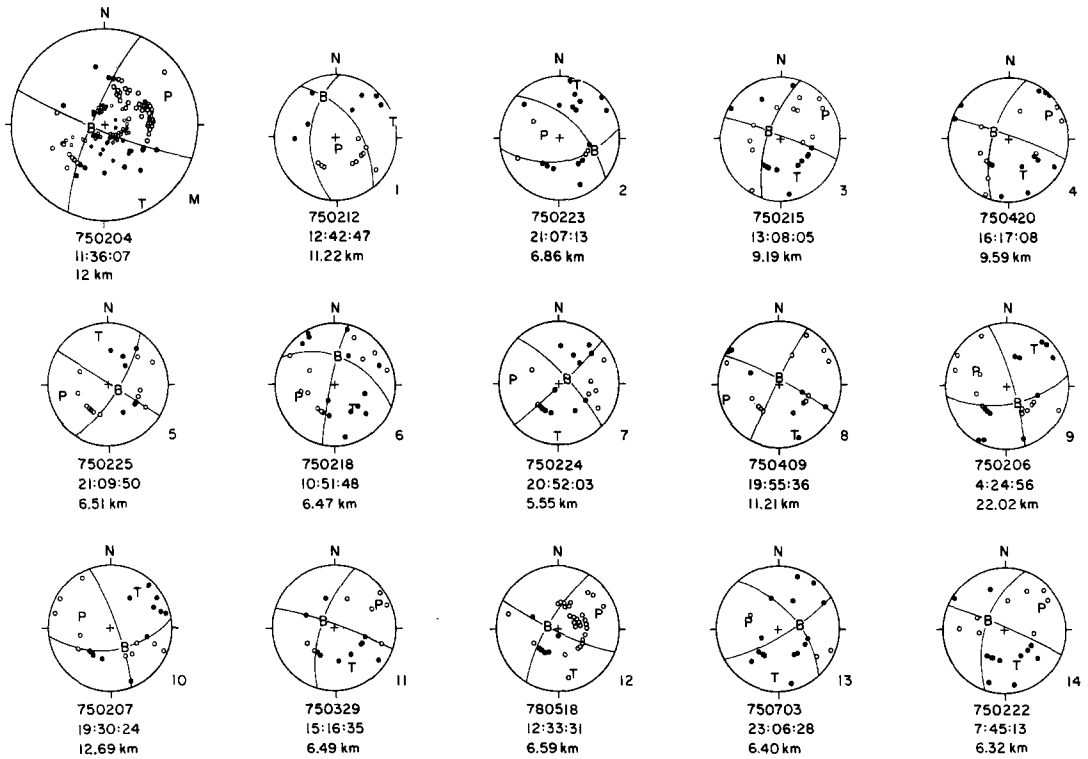

FIG. 8. First motion data for the events shown in Figure 7. Depths and origin times listed were determined by this study except for the main shock. First motion data taken from Gu *et al.* (1976) and Yuzo *et al.* (1983). Closed circles are compressions and open circles are dilatations. The projection is lower hemisphere.

model change, we compared the locations from the simultaneous inversion scheme to the locations given by HYPOINVERSE using the changed velocity model. As the layer velocities decreased, so did the travel-time residuals associated with TAI. When our chosen final velocity model (or model B) was used, the travel-time residuals for station TAI were as small as those for the other stations and the readings were not rejected. Thus, we think that the upper mantle P-wave velocity of 7.6 ± 0.09 km/sec is probably valid for the mantle beneath the entire Bohai.

The crustal P-wave values are lower than those of average continental crust, but very similar to values found in the surrounding areas. In a study of the three-dimensional P-wave velocity structure under the Beijing region 400 km southwest of Haicheng, Jin *et al.* (1980) found the P-wave velocity in the upper crust to be

5.45 and 6.47 km/sec in the lower crust. The upper mantle P-wave velocity was found to be 7.94 km/sec with the Moho at 35 km. Allowing for crustal thinning to the northeast, a valid assumption in this part of Asia, the final velocity model for the Haicheng region is consistent with that found by Jin *et al.* for the Beijing region. To the east, the crustal velocity structure of northeastern Japan is quite similar as well (Research Group for Explosion Seismology, 1977). Under Honshu, the Moho is at about 30 km, separating a lower crustal layer with $V_p = 6.6$ km/sec from an upper mantle layer with $V_p = 7.53$ km/sec.

Inversion with different depths of interfaces indicate that the depth to the Moho for the Haicheng region is between 31.0 and 32.5 km. We checked this depth range using the program Hypoinverse as well as our own method. The uncertainties of aftershock locations using HYPOINVERSE consistently are larger than those using the simultaneous inversion. Nevertheless, the locations given by HYPOINVERSE always lie within the error ellipses associated with the simultaneous inversion. Thus, we infer that the velocity model used in the inversion is appropriate throughout the station array and that the depth to the Moho is approximately 31.0 to 32.5 km beneath the entire Bohai. This thin crust beneath the Bohai is also evident in contours of depth of the Moho inferred from gravity anomalies (Wang and Liu, 1976; Tang, 1982) which indicate depths of 38 to 42 km for both the Jiaoliao uplift and the Yan Mountains flanking shallower depths for the North China Basin group. A possible explanation for both the thin crust and the low velocities found in the Xialiao-Jiaoliao transition zone is crustal extension with upwelling of hot upper mantle in the Xialiao depression.

Summary

We applied an ATD method that utilizes refracted and direct arrivals from a homogeneously layered earth model to determine simultaneously both relative locations of the Haicheng aftershock sequence and *in situ* seismic velocities. The aftershocks occurred in a west-northwest trending zone approximately 70 km x 25 km that encompasses two sets of orthogonal faults. Aftershock locations define no clear linear patterns within this zone. The trend of the aftershock zone is perpendicular to the northeast-southwest structural trend of the region. The velocity structure for the region indicates a thin crust of approximately 31 to 32.5 km. The P-wave velocities are 5.7 ± 0.1 km/sec in the upper crust, 6.6 ± 0.1 km/sec in the lower crust, and 7.6 ± 0.1 km/sec in the upper mantle beneath the Xialiao depression and the Bohai.

Acknowledgments

We are grateful to K. Aki, S. Cohn, R. McCaffrey, P. Molnar, S. Roecker, R. Stewart, and R. Wesson for their thought-provoking questions and discussions with us. We are also grateful to Gu Gongxu and Xu Shaoxie of the Institute of Geophysics, State Seismological Bureau, Beijing, People's Republic of China, for their encouragement and patience, and for making this work possible. We also wish to thank X. Jiang, the Liaoning Provincial Seismological Bureau, G. Wei, and the Shadong Provincial Seismological Bureau for making us feel so welcome and for sharing their data with us. We also wish to thank S. Luria for her assistance in the preparation of this manuscript, and R. Ricotta and P. McDowell for drafting the figures.

References

Aki, K. and W. H. K. Lee (1976). Determination of three-dimensional velocity anomalies under a seismic array using first P-arrival times from local earthquakes. 1. A homogeneous initial model, *J. Geophys. Res.* **81**, 4381–4399.

Aki, K. and P. Richards (1980). *Quantitative Seismology: Theory and Methods*, II, W. H. Freeman, San Francisco, California, 932 pp.

Cipar, J. (1979). Source processes of the Haicheng, China, earthquake from observations of *P* and *S* waves, *Bull. Seism. Soc. Am.* **69**, 1903–16.

Crosson, R. S. (1976). Crustal structure modelling of earthquake data, *J. Geophys. Res.* **81**, 3036–3054.

DeGroot, M. H. (1975). *Probability and Statistics*, Addison-Wesley, Reading, Pennsylvania, 607 pp.

Evernden, J. F. (1980). Notes on BERQ85 and associated programs, *U.S. Geol. Surv. Open-File Rept. 80-1236*, 35 pp.

Fang, Z., F. Ji, H. Jiang, and M. Ding (1976). The characteristics of Quaternary movements along the middle segment of the old Tancheng-Lujiang fracture zone and their seismogeologic conditions (in Chinese), *Scientia Geol. Sin.* **10**, 354–368.

Fitch, T. J. (1975). Compressional velocity in source regions of deep earthquakes: an application of the master earthquake technique, *Earth Planet. Sci. Letters* **26**, 156–166.

Gu, H., Y. Chen, X. Gao, and Y. Zhao (1976). Focal mechanism of Haicheng, Liaoning Province, earthquake of February 4, 1975 (in Chinese), *Acta Geophys. Sin.* **19**, 285–293.

Hsu, S. (1976). Characterizations of the Haicheng earthquake of 1975, in *Proceedings of the Lectures by the Seismological Delegation to the Peoples Republic of China*, Paul M. Muller, Editor, JPL-CIT.

Jin, A., F. Liu, and Y. Sun (1980). Three-dimensional *P* velocity structure of the crust and upper mantle under Beijing region (in Chinese), *Acta. Geophys. Sin.* **23**, 172–182.

Jones, L. M., B. Q. Wang, S. X. Xu, and T. Fitch (1982). The foreshock sequence of the 4 February 1975 Haicheng earthquake ($M = 7.3$), *J. Geophys. Res.* **87**, 4575–4584.

King, G. C. P. and G. Yielding (1984). The evolution of a thrust fault system: processes of rupture initiation, propagation and termination in the 1980 El Asnam (Algeria) earthquake, *Geophys. J. Roy. Astr. Soc.* **77**, 915–933.

Klein, F. W. (1978). HYPOINVERSE, *U.S. Geol. Surv., Open-File Rept. 78–694*, 68 pp.

Pavlis, G. L. and J. R. Booker (1980). The mixed discrete-continuous inverse problem: application to the simultaneous determination of earthquake hypocenters and velocity structure, *J. Geophys. Res.* **85**, 4801–4810.

Research Group for Explosion Seismology (1977). Regionality of the upper mantle around northeastern Japan as derived from explosion seismic observations and its seismological implications, *Tectonophysics* **37**, 117–130.

Roecker, S. W. (1982). Velocity structure of the Pamir-Hindu Kush region: possible evidence of subducted crust, *J. Geophys. Res.* **87**, 945–959, 1982.

Roecker, S. W. (1983). A hybrid method for determining relative relocations and in-situ elastic wave velocities in subducted slabs, *Earthquake Notes* **54**, 29.

Shedlock, K. M. and S. W. Roecker (1985). Determination of elastic wave velocity and relative hypocenter locations using refracted waves. I. Methodology, *Bull. Seism. Soc. Am.* **75**, 415–426.

Shedlock, K. M., S. Hellinger, and H. Ye (1985). Evolution of the Xialiao depression, *Tectonics* (in press).

Soufleris, C., J. A. Jackson, G. C. P. King, C. P. Spencer, and C. H. Scholz (1982). The 1982 earthquake sequence near Thessaloniki (Northern Greece), *Geophys. J. Roy. Astr. Soc.* **68**, 429–458.

Tang, Z. (1982). Tectonic features of oil and gas basins in eastern part of China, *Am. Assoc. Petrol. Geol.* **66**, 509–521.

Thurber, C. H. (1981). Earth structure and earthquake locations in the Coyote Lake area, central California, *Ph.D. Thesis*, Massachusetts Institute of Technology, Cambridge, Massachusetts, 322 pp.

Wang, C. and Y. Liu (1976). Framework of the crustal structure of the southern part of Liaoning Province (in Chinese), *Acta. Geophys. Sin.* **19**, 165–176.

Wu, K., M. Yue, H. Wu, X. Cao, H. Chen, W. Huang, K. Tian, and S. Lu (1976). Certain characteristics of Haicheng earthquake ($M = 7.3$) sequence (in Chinese), *Acta. Geophys. Sin.* **19**, 95–109. (English translation, *Chin. Geophys.* **1**, 289–308, 1978).

Ye, H., K. M. Shedlock, S. J. Hellinger, and J. G. Sclater (1985). The North China basin: an example of a multiply stretched intraplate basin, *Tectonics* (in press).

Yuzo, I., C. Zhu, and T. Cao (1983). On some characteristics of strong aftershocks of the 1976 (Tangshan, 1975 Haicheng, and 1976 Yangyuan-Ningling earthquakes (in Chinese), *Acta. Seism. Sin.* **5**, 15–30.

U.S. GEOLOGICAL SURVEY
BOX 25046, MS 966
DENVER FEDERAL CENTER
DENVER, COLORADO 80225 (K.M.S.)

DEPARTMENT OF EARTH, ATMOSPHERIC AND PLANETARY SCIENCES
MASSACHUSETTS INSTITUTE OF TECHNOLOGY
CAMBRIDGE, MASSACHUSETTS 02139 (K.M.S.)

U.S. GEOLOGICAL SURVEY
SEISMOLOGY LABORATORY
CALIFORNIA INSTITUTE OF TECHNOLOGY
PASADENA, CALIFORNIA 91125 (L.M.J.)

INSTITUTE OF GEOPHYSICS
STATE SEISMOLOGICAL BUREAU
BEIJING, PEOPLE'S REPUBLIC OF CHINA (M.X.)

Manuscript received 4 June 1984